J Nanopart Res (2014) 16:2240
DOI 10.1007/s11051-013-2240-y

RESEARCH PAPER

Si nanoparticles fabricated from Si swarf by photochemical etching method

Taketoshi Matsumoto · Masanori Maeda · Junichi Furukawa · Woo Byoung Kim · Hikaru Kobayashi

Received: 3 July 2013 / Accepted: 30 December 2013 / Published online: 27 February 2014

Abstract Si nanoparticles are produced from Si swarf which is a waste during slicing Si ingots to produce Si wafers for solar cell use. The beads mill method produces flake-like Si with scores of nanometers width from Si swarf. Subsequent photochemical dissolution with light longer than 560 nm wavelength in a 0.5 % HF solution results in sphere-shaped Si nanoparticles of 1–7 nm diameter. Si nanoparticles dispersed in ethanol show blue photoluminescence at ~400 nm (3.1 eV) under UV irradiation, indicating band-gap widening due to the quantum confinement effect. The band-gap energy of most of the Si nanoparticles is estimated to be 2.5–3.3 eV from the PL spectra, corresponding to the Si nanoparticle size of 1.9–3.2 nm. On the other hand, Si nanoparticles produced by immersion in the HF solution in the dark show much weaker blue photoluminescence. These results demonstrate that the Si dissolution reaction is greatly enhanced by photo-generated holes.

T. Matsumoto · M. Maeda · J. Furukawa · H. Kobayashi (✉)
Institute of Scientific and Industrial Research, Osaka University, 8-1 Mihogaoka, Ibaraki, Osaka 567-0047, Japan
e-mail: h.kobayashi@sanken.osaka-u.ac.jp

W. B. Kim
Department of Energy Engineering, DanKoook University, San 29, Anseo-dong, Cheonan-si, Chungcheongnam-do 330-714, Korea

Keywords Silicon · Nanoparticles · Swarf · Photoluminescence · UV/Vis spectroscopy · Transmission electron microscopy · Energy conversion and storage

Introduction

Si nanoparticles have excellent characteristics such as wide band-gap due to quantum confinement effect, huge surface area, and active surface atoms with low coordination numbers. Extensive studies have been made in order to apply Si nanoparticles to tandem solar cells (Conibeer 2010), photodetectors (Ramizy et al. 2011), sensors (Kang et al. 2011), Li ion battery anodes (Morita and Takami 2006), memories (Tsoukalas et al. 2005), and hydrogen source (Erogbogbo et al. 2013). Various methods have been developed for fabrication of Si nanoparticles including pyrolysis of silane gas, chemical vapor deposition (CVD), disproportionation reaction of SiO_x, Zintl reaction, LiAlH reduction of $SiCl_4$, supercritical fluid, ultrasonication of anodized Si (Kang et al. 2011), electroreduction of $SiCl_4$ (Aihara et al. 2001), arc-discharge (Liu et al. 2005), ion implantation (White et al. 1996), laser ablation (Watanabe et al. 2002), and milling bulk Si (Verdoni et al. 2011). However, it is difficult to produce size-controlled Si nanoparticles under low fabrication cost. Mass fabrication is also difficult using these methods.

In order to reduce the production cost of crystalline Si solar cells, the thickness of Si wafers has been decreased, and during production of 180 μm thick Si wafers currently used for solar cell production, nearly the same weight of Si swarf, which is disposed as industrial waste, is generated. Therefore, development of technologies to use Si swarf will give promising breakthrough for a vast decrease in cost of solar cells, Li ion batteries, etc.

In the present study, we have developed a method of fabricating Si nanoparticles from Si swarf using a simple method, i.e., beads mill plus photochemical etching method. Produced Si nanoparticles possess the size distribution maximum at 4.2–7.5 nm. The Si nanoparticles in filtrate exhibit photoluminescence (PL) at ~400 nm, indicating band-gap widening due to the quantum confinement effect (Bulutay and Ossicini 2010; Wilcoxon et al. 1999; Azuma and Saito 2011; Conibeer 2010). The corresponding size is estimated to be 1.9–3.2 nm.

Experimental

Materials

Si swarf produced during production of solar cell grade boron-doped p-type wafers by slicing Si ingots was used as a starting material to form Si nanoparticles. Coolant included in Si swarf was removed by ultrasonic cleaning in a mixture of *N*-methyl-2-pyrrolidinone (Wako Chemicals, SC grade) and acetone (Kanto Chemicals, EL grade).

Si swarf was milled by a ball mill with alumina balls of a 1 mm diameter, followed by milling with Ashizawa Fintech LMZ015 (zirconia beads of a 0.3 mm diameter, Nikkato) and Nano Getter DMS615 (zirconia beads of a 0.05 mm diameter, Nikkato) beads mill apparatuses.

Figure 1 shows the process flow for fabrication of Si nanoparticles from Si swarf by use of the photochemical etching method. Si nanoparticles were grounded with a nano getter beads mill. Then, they were immersed in a hydrogen fluoride (HF, ultra high purity hydrofluoric acid, Stera Chemifa) aqueous solution (0.5 %) diluted by an ultra-pure water with stirring. The yield of Si nanoparticles was maximum at the HF concentration of 0.5 % after 42 h photochemical dissolution. During immersion, light from the

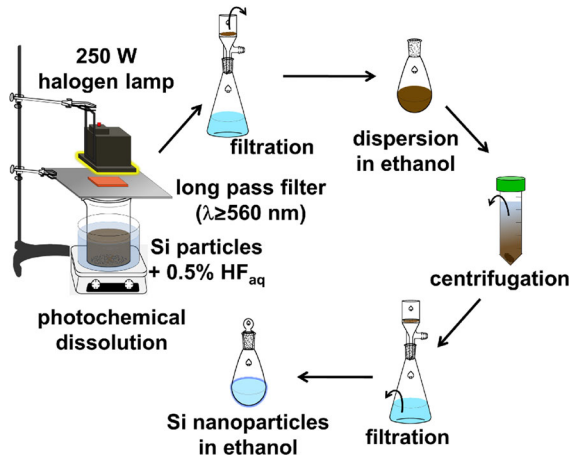

Fig. 1 Process flow for the formation of Si nanoparticles from Si swarf

halogen lamp with wavelength longer than 560 nm was irradiated for 6 and 42 h. The wavelength full width at half maximum of the light from the halogen lamp was ~1,500 nm with the peak top at ~1,000 nm. The photon flux in the wavelength region 560–1,127 nm was roughly estimated to be 8×10^{18} s^{-1} for the light irradiated area of 16 cm^2. The solution temperature rose up to ~40 °C during light irradiation. Aggregated Si nanoparticles were filtered and rinsed with ultra-pure water with suction filtering to remove HF. Si nanoparticles were dispersed in ethanol and centrifuged to remove aggregated or large Si nanoparticles. The supernatant liquid was filtered with a membrane filter having a 100 nm pore diameter.

Instrument and characterization

The amount of incorporated coolant was determined using a thermogravimetry (Rigaku TG8120) and a differential thermal analysis apparatus (DTA, Rigaku DSC 8270). The size distribution of Si particles was measured by a laser diffraction particle size analyzer (Shimadzu SALD-2200), an X-ray diffraction (XRD) apparatus (Rigaku RINT-2500), and a transmission electron microscope (TEM) at an incident electron energy of 300 keV (JEOL JEM-3000F). PL spectra of Si nanoparticles were measured using a Hitachi Hi-Tech F-7000 fluorescence spectrometer. Absorption spectra were recorded with a JASCO V-570 UV–Vis spectrometer.

Results and discussion

Removal of coolant from Si swarf

Figure 2 shows the TG–DTA curves for Si swarf before and after cleaning with the mixture of *N*-methyl-2-pyrrolidinone and acetone. Before cleaning (Fig. 2a), mass-loss was observed at temperatures below 200 °C, and endothermic peaks at 90 and 160 °C and an exothermic peak at ~280 °C appeared in the DTA curve. These phenomena can be assigned to desorption and oxidation of coolant. After cleaning (Fig. 2b), no significant structures were found in the TG and DTA curves, indicating effective removal of coolants. The slight increase of the weight with the increase of temperature is thought to be due to oxidation of Si nanoparticles promoted by low concentration contaminants such as Fe, Ni, and Zn (materials of wire saw).

Formation of Si nanoparticles from Si swarf with photochemical etching method

A laser diffraction particle size analyzer indicated that the diameter of the Si swarf was in the range between 300 nm and 4 μm. To fabricate Si nanoparticles, the photochemical etching method was employed after

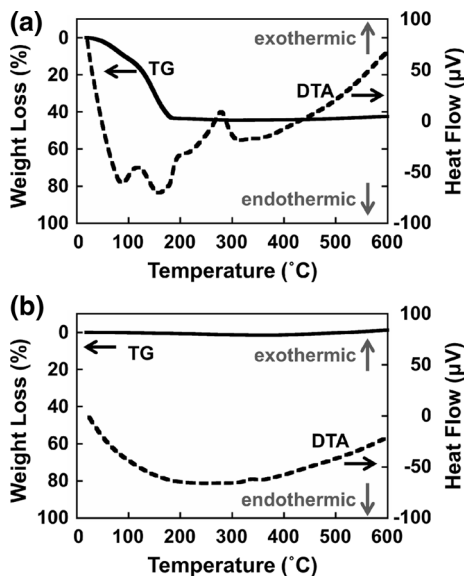

Fig. 2 TG and DTA spectra for Si swarf **a** before and **b** after cleaning with the mixture of *N*-methyl-2-pyrrolidinone and acetone

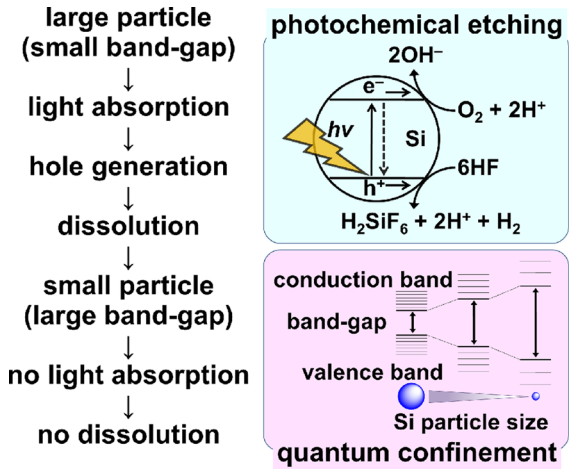

Fig. 3 Formation mechanism of Si nanoparticles by use of the photochemical etching method

beads milling. When light filtered with a long-pass filter is irradiated on Si nanoparticles, they absorb light unless the photon energy is lower than the band-gap of Si nanoparticles, leading to generation of electron–hole pairs (Fig. 3). In the dark, no substantial reaction occurs in an HF solution, while photo-irradiation causes the following photochemical etching reaction using photo-generated holes, h^+, trapped at surface Si atoms (Lianto et al. 2012, Zgang 2001, Kolasinski 2003):

$$Si + 4h^+ + 4F^- \rightarrow SiF_4, \quad (1)$$

$$SiF_4 + 2HF \rightarrow H_2SiF_6, \quad (2)$$

$$4H^+ + 4e^- \rightarrow 2H_2. \quad (3)$$

The band-gap of Si nanoparticles smaller than ~10 nm increases with a decrease in the diameter due to the quantum confinement effect (Bulutay and Ossicini 2010; Wilcoxon et al. 1999; Azuma and Saito 2011; Conibeer 2010). Incident light is not absorbed any more when the band-gap of Si nanoparticles becomes larger by photochemical dissolution than the energy of incident photons.

Figure 4 shows the XRD patterns for Si swarf and Si nanoparticles filtered out from the solution of Si swarf after ball milling followed by beads milling with 0.3 mm beads, after beads milling with 0.05 mm beads and after photochemical dissolution for 42 h. Observed peaks are attributable to Si(111) (28.4° peak), Si(220) (47.4° peak), Si(311) (56.2° peak), Si(400) (69.2° peak), Si(331) (76.4° peak), and Si(422) (88.0° peak). A small peak at 26.4° is due to

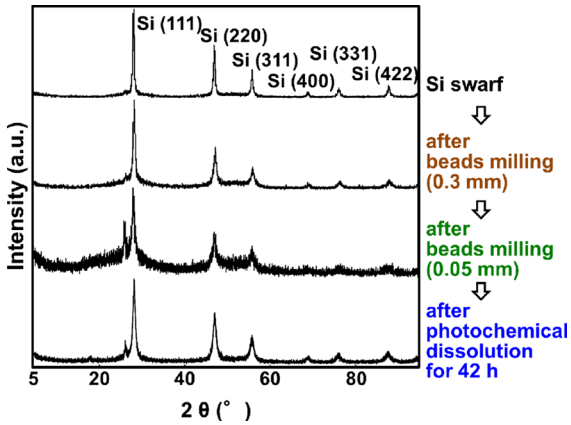

Fig. 4 XRD patterns of Si nanoparticles filtered out from the solution of Si swarf after milling and subsequent photochemical dissolution. The XRD pattern for Si swarf is shown in the top for reference

graphite used as a base to hold Si ingots during slicing process. Graphite was concentrated with repeated filtration after each milling process.

Figure 5 shows the size distributions of Si swarf and Si nanoparticles estimated from the main (111) and (220) XRD peaks shown in Fig. 4 using an algorithm proposed by Ida et al. (2006). The photochemical etching method resulted in sharp peaks for both (111) and (220) orientations, and the mode diameter was estimated to be 4.2 and 7.5 nm for the (111) and (220) orientations, respectively.

Figure 6a shows the transmission electron micrograph TEM of Si nanoparticles produced by milling. Aggregated flake-like structures of a few hundred nanometers and Si nanoparticles of a few nanometers were observed. Figure 6b shows the TEM micrograph of Si nanoparticles in filtrate after photochemical dissolution for 42 h. The Si nanoparticles were spherical, and the diameter was in the range between 1 and 7 nm. Lattice images are clearly seen and the lattice fringe spacing was ~0.314 nm, corresponding to spacing for the Si(111) plane. The size of Si nanoparticles observed by TEM micrography agrees with those determined from XRD measurements (Fig. 5).

PL and UV–Vis absorption spectra of Si nanoparticles

PL spectra for Si nanoparticles are shown in Fig. 7. The wavelength of excitation light was 300 nm

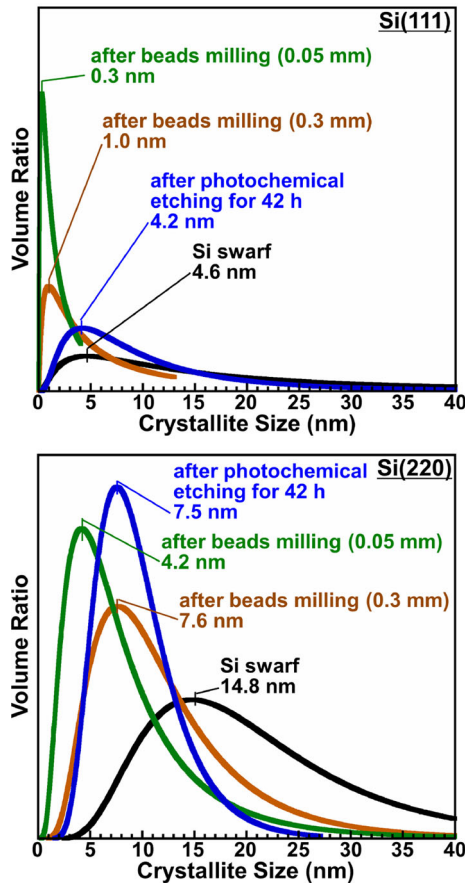

Fig. 5 Distribution of Si nanoparticle diameter estimated from the Si(111) and Si(220) XRD peaks in Fig. 4

(4.1 eV). A PL peak was observed in the range between 380 nm (3.3 eV) and 500 nm (2.5 eV) with a peak top at ~400 nm (~3.1 eV, violet color) and its intensity increased with the photochemical etching time. These results indicate that Si nanoparticles with band-gap higher than the PL energy were formed by the photochemical etching method.

Using the effective mass approximation (EMA) method, the band-gap energy, E_{gap}, of spherical Si nanoparticles is given by

$$E_{gap} = E_{bulk} + \frac{h^2}{2\mu D^2}, \quad (4)$$

where E_{bulk} is the band-gap energy of bulk Si, h is a Plank's constant, μ is the reduced mass of an electron–hole pair, and D is the diameter of Si nanoparticles (Conibeer 2010; Woggon 1997). μ is estimated to be 0.19 m_0 from the weighted average of the effective

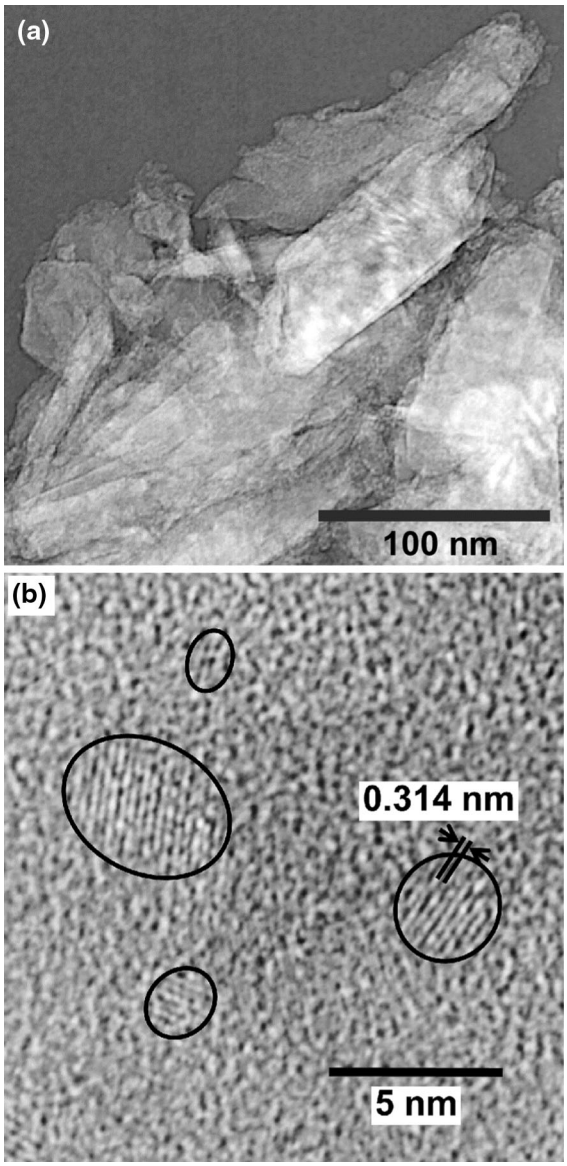

Fig. 6 TEM micrographs of Si nanoparticles in filtrate. The Si nanoparticles were fabricated from Si swarf by use of the following methods: **a** milling; **b** subsequent photochemical etching for 42 h

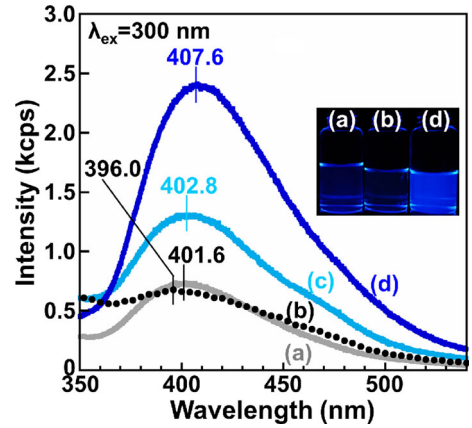

Fig. 7 PL spectra of ethanol solutions containing Si nanoparticles before etching (filtered Si swarf) (*a*), after immersion in an HF solution for 42 h in the *dark* (*b*), and after photochemical dissolution for 6 h (*c*) and 42 h (*d*). The inserted photographs show *blue* PL for the ethanol solutions *a*, *b*, and *d* under UV irradiation of 365 nm wavelength light. (Color figure online)

mass of electrons and holes of bulk Si where m_0 is the electron rest mass (Kux et al. 1995). Azuma and Saito, on the other hand, obtained the reduced mass of 0.11 m_0 from a relationship of the PL energy versus the fabricated Si nanoparticle size (Azuma and Saito 2011). Using these values, sizes of Si nanoparticles showing blue PL are estimated to be 1.9–3.2 nm from the PL energy (380 nm or 3.3 eV–500 nm or 2.5 eV). Si nanoparticles of these sizes were certainly observed by TEM (Fig. 6) and XRD (Fig. 5).

Blue PL for Si nanoparticles and porous Si has been reported in previous literature, and the excitation and relaxation mechanism is related to quantum confinement effect (Bulutay and Ossicini 2010; Wilcoxon et al. 1999; Azuma and Saito 2011; Conibeer 2010). Defect states in SiO_2 on Si nanoparticles and interface states at SiO_2/Si nanoparticles interface are also considered to play a role in PL (Yang et al. 2011; Lin and Chen 2009). Figure 8 shows plots of the PL energy versus the Si nanoparticle size in previous papers and curves calculated with the EMA methods. The PL energy of Si nanoparticles decreases with the Si nanoparticle size, and reasonably fits to the EMA curves. Some of PL energies of small Si nanoparticles are lower than the EMA calculation presumably due to the presence of surface and interface states as described in previous literature (Wilcoxon et al. 1999; Wolkin et al. 1999). Figure 8 can lead to the conclusion that blue PL from Si nanoparticles arises from band-gap widening due to the quantum confinement effect.

Figure 9 shows the UV–Vis absorption spectra for supernatant liquid of ethanol solutions including Si swarf (a), and Si nanoparticles before etching (b), after immersion in an HF solution for 42 h in the dark (c), and after photochemical dissolution for 6 h (d) and 42 h (e). A broad absorption feature was present for Si

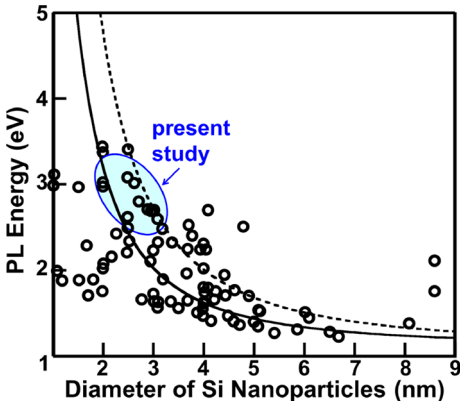

Fig. 8 Plots of the band-gap of Si nanoparticles versus the diameter including results reported previously (Wilcoxon et al. 1999; Conibeer 2010; Azuma and Saito 2011; Kolasinski 2003; Yang et al. 2011; Holmes et al. 2001; Lin and Chen 2009). *Curves* deduced using the EMA method are shown by the *solid line* for the reduced mass of an electron–hole pair of (Conibeer 2010) and the *dashed line* for (Azuma and Saito 2011)

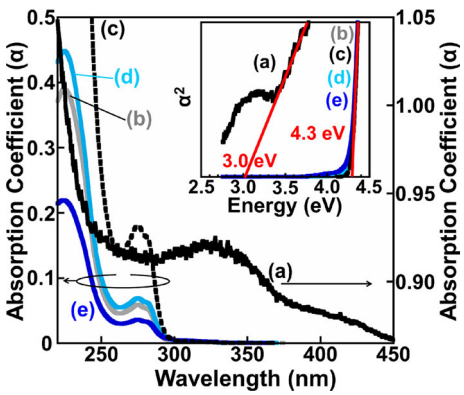

Fig. 9 UV–Vis absorption spectra of ethanol solutions containing Si swarf (*a*), and Si nanoparticles before etching (filtered Si swarf) (*b*), after immersion in an HF solution for 42 h in the *dark* (*c*), and after photochemical dissolution for 6 h (*d*), and 42 h (*e*). The *inset* shows the plot of the square of absorption coefficient versus photon energy

swarf (Fig. 9a), while a sharp rise was observed near 300 nm (4.1 eV) for Si nanoparticles (Fig. 9b–e). The optical band-gap energy, E_g, for direct transition can be determined using the following equation:

$$\alpha^2 = A(E - E_g), \tag{5}$$

where α is the absorption coefficient, A is a constant, E is the energy of incident photon (Grundmann 2010). Using Eq. (5), E_g can be determined from the intercept with the horizontal axis of the plot of α^2 versus E (inset of Fig. 9). Using this method, the direct band-gap energy for Si swarf is determined to be 3.0 eV, in reasonable agreement with the energy of direct $\Gamma_{25} \rightarrow \Gamma_{15}$ transition for crystalline Si 3.2 eV with no quantum confinement effect (Wilcoxon et al. 1999). In the case of Si nanoparticles, the band-gap energy is estimated to be 4.3 eV. These results clearly indicate band-gap widening of Si nanoparticles due to the quantum confinement effect. Moreover, the high intensity tail below 3 eV is obtained for Si swarf due to indirect excitation, while no tail is present for Si nanoparticles. This is because continuous states, i.e., band structures, resulting from infinitely periodic potential, are not formed, but discrete states are generated with decrease in size of Si nanoparticles due to small numbers of Si atoms (Bulutay and Ossicini 2010).

Conclusion

Si nanoparticles were fabricated from Si swarf by use of the milling method followed by the photochemical etching method in a 0.5 % HF solution. Detailed investigation has led to the following results and conclusion.

(1) Sphere-shaped Si nanoparticles of 1–7 nm diameter can be formed by the milling method followed by the photochemical etching method.
(2) The blue PL intensity greatly increases after photochemical dissolution, while chemical etching in the dark doesn't increase the blue PL intensity. These results demonstrate that dissolution proceeds only under irradiation.
(3) The band-gap energy of the Si nanoparticles in filtrate is estimated to be 2.5–3.3 eV from the strong blue PL, corresponding to the Si nanoparticle diameter of 1.9–3.2 nm.
(4) UV–vis measurements show that Si swarf has a considerably high optical absorption coefficient in the wavelength region longer than 300 nm, but after milling, the absorption coefficient greatly decreases. After photochemical dissolution, absorption longer than 300 nm completely disappears. These results are attributed to decrease in the size of Si nanocrystals by milling and photochemical dissolution.

Acknowledgments The authors acknowledge Professor Y. Hitomi of Doshisha University for measurements of the PL spectra.

References

Aihara S, Ishi R, Fukuhara M, Kamata N, Terunuma D, Hirano Y, Saito N, Aramata M, Kashinuma S (2001) Electroreductive synthesis and optical characterization of silicon nanoparticles. J Non-Cryst Solids 296:135–138. doi:10.1016/S0022-3093(01)00923-1

Azuma S, Saito S (2011) Regulation of Si nanoparticles through photon-enhanced chemical etching. Chem Lett 40:1294. doi:10.1246/cl.2011.1294

Bulutay C, Ossicini S (2010) Electronic and optical properties of silicon nanocrystals. In: Pavesi L, R Turan (eds) Silicon Nanocrystals. Wiley-VCH, Weinheim, pp 5–38

Conibeer G (2010) Applications of Si nanoparticles in photovoltaic solar cells silicon nanocrystals. In: Pavesi L, R Turan (eds) Silicon Nanocrystals. Wiley-VCH, Weinheim, pp 555–561

Erogbogbo F, Lin T, Tucciarone PM, LaJoie KM, Lai Patki LGD, Prasad PN, Swihart MT (2013) On-demand hydrogen generation using nanosilicon: splitting water without light, heat, or electricity. Nano Lett 13:451–456. doi:10.1021/nl304680w

Grundmann M (2010) The physics of semiconductors, 2nd edn. Springer, Berlin, pp 271–279

Holmes JD, Ziegler KJ, Doty RC, Pell LE (2001) Highly luminescent silicon nanocrystals with discrete optical transitions. J Am Chem Soc 123:3743–3748. doi:10.1021/ja002956f

Ida T, Shimazaki S, Hibino H, Toraya H (2006) Diffraction peak profiles from spherical crystallites with lognormal size distribution. J Appl Cryst 36:1107–1115. doi:10.1107/S0021889803011580

Kang Z, Liu Y, Lee S-T (2011) Small-sized silicon nanoparticles: new nanolights and nanocatalysts. Nanoscale 3:777–791. doi:10.1039/C0NR00559B

Kolasinski KW (2003) The mechanism of Si etching in fluoride solutions. Phys Chem Chem Phys 5:1270–1277. doi:10.1039/b212108e

Kux A, Kovalev D, Koch F (1995) Slow luminescence from trapped charges in oxidized porous silicon. Thin Solid Films 255:143–145. doi:10.1016/0040-6090(94)05640-Y

Lianto P, Yu S, Wu J, Thompson CV, Choi WK (2012) Vertical etching with isolated catalysts in metal-assisted chemical etching of silicon. Nanoscale 4:7359–7532. doi:10.1039/c2nr32350h

Lin S-W, Chen D-H (2009) Synthesis of water-soluble blue photoluminescent silicon nanocrystals with oxide surface passivation. Small 5:72–75. doi:10.1002/smll.200800677

Liu S-M, Kobayashi M, Sato S, Kimura K (2005) Synthesis of silicon nanowires and nanoparticles by arc-discharge in water. Chem Commun. doi:10.1039/b506995e

Morita T, Takami N (2006) Composite material as high-capacity anode material for rechargeable lithium batteries. J Electrochem Soc 153:A425–A430. doi:10.1149/1.2142295

Ramizy A, Hassan Z, Omar K, Al-Douri Y, Mahdi MA (2011) New optical features to enhance solar cell performance based on porous silicon surfaces. Appl Surf Sci 257:6112–6117. doi:10.1016/j.apsusc.2011.02.013

Tsoukalas D, Dimitrakis P, Kolliopoulou S, Normand P (2005) Recent advances in nanoparticle memories. Mater Sci Eng B 124–125:93–101. doi:10.1016/j.mseb.2005.08.105

Verdoni LP, Fink MJ, Mitchell BS (2011) Fractionation process of mechanochemically synthesized blue-green luminescent alkyl-passivated silicon nanoparticles. Chem Eng J 172:591–600. doi:10.1016/j.cej.2011.06.033

Watanabe K, Sawada K, Koshiba M, Fujii M, Hayashi S (2002) Photolumine decay-dynamics of Si nanoparticles prepared by pulsed laser ablation. Appl Surf Sci 197–198:635–638. doi:10.1016/S0169-4332(02)00431-2

White CW, Budai JD, Withrow SP, Zhu JG, Pennycock SJ (1996) Ion beam synthesis of nanocrystals and quantum dots in optical materials. In: IEEE conference proceeding, p 824

Wilcoxon JP, Samara GA, Provencio PN (1999) Optical and electronic properties of Si nanoclusters synthesized in inverse micelles. Phys Rev B 60:2704–2714. doi:10.1103/PhysRevB.60.2704

Woggon U (1997) Optical properties of semiconductor quantum dots. Springer, Berlin 3

Wolkin MV, Jorne J, Fauchet PM, Allan G, Delerue C (1999) Electronic states and luminescence in porous silicon quantum dots: the role of oxygen. Phys Rev Lett 82:197–200. doi:10.1103/PhysRevLett.82.197

Yang S, Li W, Cao B, Zeng H, Cai W (2011) Origin of blue emission from silicon nanoparticles: direct transition and interface recombination. J Phys Chem C 115:21056–21062. doi:10.1021/jp2075836

Zgang XG (2001) Electrochemistry of silicon and its oxide. Kluwer Academic Plenum, New York, p 53